

Energy levels of one and two holes in parabolic quantum dots

F. B. Pedersen

*Department of Physics and Materials Research Laboratory, University of Illinois at Urbana-Champaign, Urbana, Illinois 61801
and Institutt for Fysikk, Norges Tekniske Høgskole, N-7034 Trondheim, Norway*

Yia-Chung Chang

Department of Physics and Materials Research Laboratory, University of Illinois at Urbana-Champaign, Urbana, Illinois 61801

(Received 4 August 1995)

Calculations of energy levels of single-hole and two-hole states in a GaAs/Al_{0.3}Ga_{0.7}As parabolic quantum dot have been performed with a multiband effective-mass method. Both the valence-band degeneracy and the Coulomb interaction are taken into account using the axial approximation for the bulk band structure. The variational problem is solved with an iterative relaxation technique which allows us to use a large number of basis functions. The valence-band mixing is shown to be substantial and the Coulomb interaction between the holes leads to a resonant tunneling energy that is (in general) nonlinear with respect to the strength of the confinement potential. It is found that at sufficiently large confinement potentials, both the single-hole and two-hole ground states are changed from primarily heavy-hole-like to light-hole-like.

I. INTRODUCTION

Recent progress in nanofabrication technology has made it possible to make individual quantum dots.¹ These structures confine electrons (or holes) in all three spatial dimensions and are sometimes referred to as artificial atoms. Quantum dots grown as nanocrystallites usually have a spherical shape and a steplike confinement potential. In such preparation processes several dots are created and the interaction between individual dots may be important. This complication can be circumvented with the use of modern lithographic techniques. Through a series of masking and etching steps it is possible to make a single quantum dot starting with a quantum-well heterostructure. The resulting dot then typically has a disklike shape with a lateral confinement potential (from band bending) that to a good approximation is parabolic.² In such quantum dots the gate potential of the dot can be controlled at will, giving unprecedented control of the number of electrons on the dot. The spectroscopic study of these nanostructures has been facilitated by the recent development of techniques that allow the measurement of energy levels of a single quantum dot containing N ($N=1,2,3, \dots$) electrons.^{3,4} Few-electron systems in quantum dots have been considered theoretically by several authors.⁵⁻⁹ The early study by Bryant emphasized the importance of electron-electron correlations, as the confinement energy and Coulomb energies are comparable in magnitude. As opposed to larger dots with many electrons, these small dots can consequently not be described semiclassically in terms of single-particle energies plus a constant charging energy to account for the Coulomb interaction. The theoretical studies have therefore employed a full numerical diagonalization, taking the Coulomb energy fully into account. These studies have been numerically demanding and limited to just a few electrons (Kumar, Laux, and Stern⁹ treated up to 10 electrons self-consistently within the Hartree approximation.)

Despite the complex energy structure of the parabolic

quantum dots, the far-infrared (FIR) absorption spectrum turned out to be remarkably simple; dominated by only two peaks and being essentially independent of the number of electrons on the dot and the electron-electron interaction. It was shown that this was a consequence of the parabolic confinement potential, which allows for the separation of the center-of-mass and relative motion. As the dipole field only couples to the center-of-mass motion, the FIR absorption experiments see only features at the single-particle energies. This is the generalized Kohn's theorem to our knowledge.^{6,7,10-12}

In the present work we consider a parabolic quantum dot containing holes rather than electrons. Although to our knowledge no experimental work is yet reported for such dots, it is expected that they will have more interesting features as Kohn's theorem is violated due to the strong mixing between the valence bands¹³⁻¹⁵ and the effect of interparticle correlation on the energy levels can be probed experimentally. In our work we study a GaAs quantum dot, prepared from a GaAs/Al_{0.3}Ga_{0.7}As [001] quantum well. Whereas disklike quantum dots containing electrons to a good approximation can be considered as two dimensional, this is not the case if the dot is occupied by holes. The (relatively) small splitting between the heavy- and light-hole bands makes it necessary to include several subbands in the treatment. (The effect of the finite width of the quantum well is further enhanced by the holes' smaller Bohr radius compared to electrons.) In our study we consequently take into account several subbands. Furthermore, the effect of the *finite* barrier height is accounted for in an approximate way. Expanding the wave function in a large basis we calculate variationally the low-lying energy levels for a parabolic quantum dot containing one or two holes. While the single-hole problem can be treated using a standard numerical diagonalization technique, we use instead an iterative relaxation technique for the two-hole problem because of the large number of basis functions needed.

In Sec. II we present the model used and construct appro-

appropriate basis functions for the single- and two-hole problem. A brief account of the calculation problem is given in Sec. III. The numerical results are presented in Sec. IV for the single-hole and two-hole cases separately. A short summary is finally left for Sec. V.

II. GENERAL THEORY

This section contains the theoretical background for the problem and is divided into three parts. First we present the Hamiltonian used, then we construct appropriate basis states for the single-hole and two-hole problem.

A. Model

Bulk GaAs has the symmetry of the tetrahedral point group T_d . In these zinc-blende crystals the valence states are p like and transform as the Γ_5 representation of T_d , whereas the $s = \frac{1}{2}$ spinor transforms like Γ_6 . The spin-orbit interaction is diagonal in the direct-product space of these representations. Since group theory gives that $\Gamma_5 \times \Gamma_6 = \Gamma_7 + \Gamma_8$ we see that the spin-orbit interaction splits the sixfold degenerate valence-band edge into a Γ_8 and a Γ_7 state. The Γ_8 states are fourfold degenerate at $\mathbf{k}=0$, while splitting into the twofold Kramer's degenerate heavy- and light-hole bands for non-zero \mathbf{k} . The Γ_7 states correspond to the split-off band, which is twofold degenerate at $\mathbf{k}=0$. The direct-product basis (spin-orbit coupled basis) is such that the angular momentum $\mathbf{J} = \mathbf{L} + \mathbf{S}$ and its projection along the z axis are diagonal. The p -like valence states have $L=1$, giving $J = \frac{3}{2}$ or $J = \frac{1}{2}$. The former is the Γ_8 quadruplet, the latter the Γ_7 -like split-off band. In GaAs the split-off band lies an energy 0.35 eV below the Γ_8 states at $\mathbf{k}=0$, and it is therefore a good approximation to assume that these states are completely decoupled from the Γ_8 quadruplet. We will therefore ignore the split-off band in our treatment of the hole states.

In the limit of decoupled split-off band, the hole is pictured as a spin- $\frac{3}{2}$ particle with four components $j_z = (\frac{3}{2}, \frac{1}{2}, -\frac{1}{2}, -\frac{3}{2})$. In the effective-mass approximation the kinetic energy of the hole is then described in this basis by the 4×4 Kohn-Luttinger Hamiltonian¹⁶

$$H_{KL} = \frac{\hbar^2}{2m_0} \begin{bmatrix} H_h & R & S & 0 \\ R^* & H_l & 0 & S \\ S^* & 0 & H_l & -R \\ 0 & S^* & -R^* & H_h \end{bmatrix}, \quad (1)$$

where¹⁷

$$\begin{aligned} H_h &= (\gamma_1 + \gamma_2)(k_x^2 + k_y^2) + (\gamma_1 - 2\gamma_2)k_z^2, \\ H_l &= (\gamma_1 - \gamma_2)(k_x^2 + k_y^2) + (\gamma_1 + 2\gamma_2)k_z^2, \\ R &= 2\sqrt{3}\gamma_3 ik_- k_z, \\ S &= \sqrt{3}\gamma k_-^2 + \sqrt{3}\mu k_+^2, \end{aligned} \quad (2)$$

and

$$\mathbf{k} = -i\nabla, \quad (3)$$

$$k_{\pm} = k_x \pm ik_y.$$

As usual γ_1, γ_2 , and γ_3 are the Luttinger parameters and $\gamma = \frac{1}{2}(\gamma_2 + \gamma_3), \mu = \frac{1}{2}(\gamma_2 - \gamma_3)$. We have neglected the small linear terms in the Kohn-Luttinger Hamiltonian that are present because GaAs lacks inversion symmetry.

The quantum-well potential in the z direction is due to the offset between the valence-band edges in the well and barrier materials. The presence of the quantum well lowers the symmetry of the problem from T_d to D_{2d} . This symmetry-reduction results in a splitting of the heavy- and light-hole states at $\mathbf{k}=0$. We model this by a finite potential well of width w :

$$V_{\perp}(z) = \begin{cases} \Delta E_v, & |z| \geq w/2 \\ 0, & |z| < w/2. \end{cases} \quad (4)$$

The lateral confinement potential is parabolic, viz.,

$$V_{\parallel}(\rho) = \frac{1}{2}K\rho^2 \quad (5)$$

in cylindrical coordinates. Here K is a constant measuring the strength of the potential. The hole-hole interaction is modeled by a statically screened Coulomb potential:

$$V(\mathbf{r}_1, \mathbf{r}_2) = \frac{e^2}{4\pi\epsilon|\mathbf{r}_2 - \mathbf{r}_1|}. \quad (6)$$

To simplify the calculations without substantial loss of accuracy we will adopt the axial approximation,¹⁸ which in the present model amounts to putting $\mu=0$. The axial approximation corresponds to ignoring the cubic terms that are not axially symmetric about the z axis. The accuracy of the axial model can be assessed by the smallness (relative to 1) of the parameter $\delta = (\gamma_3 - \gamma_2)/\gamma_1$. For GaAs $\delta=0.11$. Since in general the warping terms are second order in δ , the axial approximation should be well justified in GaAs. Other studies also confirm this conclusion.¹⁹ Having presented the Hamiltonian for the problem we now go on to construct basis states appropriate for the variational calculation.

B. Single-hole basis

With only one hole in the quantum dot the Hamiltonian is

$$H = H_{KL} + V_{\parallel}(\rho) + V_{\perp}(z). \quad (7)$$

In the Kohn-Luttinger representation the single-hole wave function is expressed as

$$\psi(\mathbf{r}) = \sum_{j_z} F^{j_z}(\mathbf{r}) \left| \frac{3}{2}, j_z \right\rangle, \quad (8)$$

where $j_z = \pm \frac{3}{2}, \pm \frac{1}{2}$, $|\frac{3}{2}, j_z\rangle$ is the (spin-orbit coupled) band-edge Bloch function, and $F(\mathbf{r})$ is the envelope function. Since the confinement potential has cylindrical symmetry the envelopes will have a definite angular momentum. Define therefore a *total* angular momentum \mathbf{F} as

$$\mathbf{F} = \mathbf{J} + \mathbf{L}, \quad (9)$$

where \mathbf{J} is the angular momentum of the Bloch function and \mathbf{L} the envelope angular momentum. In the axial approximation \mathbf{F}_z is a constant of the motion and it is possible to find

simultaneous eigenstates of the Hamiltonian H and \mathbf{F}_z . We label the eigenstates of H by f_z (a good quantum number) and states with different f_z will not be coupled by the Hamiltonian.²⁰ A general hole state can consequently be written as

$$\psi(\mathbf{r}) = \sum_{j_z} F^{j_z}(\rho, z) e^{i\phi(f_z - j_z)|\frac{3}{2}, j_z\rangle}. \quad (10)$$

Next we must find a suitable basis appropriate for the expansion of the hole envelopes. If band mixing is neglected ($R=S=0$) the Kohn-Luttinger Hamiltonian becomes diagonal and the heavy- and light-hole states become uncoupled. This diagonal problem is separable in an in-plane and a subband part whose solution is of the form

$$\phi_{nls}(\mathbf{r}) = \Phi_{nl}(\rho, \phi) f_s(z), \quad (11)$$

where $\Phi_{nl}(\rho, z)$ is the 2D harmonic oscillator and $f_s(z)$ the s th subband function. Explicitly the eigenfunctions of the 2D oscillator can be written in cylindrical coordinates as

$$\Phi_{nl}(\rho, \phi) = C_{nl}(i\rho)^{|l|} e^{-\rho^2/2a^2} e^{il\phi} L_n^{|l|}(\rho^2/a^2). \quad (12)$$

Here L_n^l is the generalized Laguerre polynomial and the normalization constant C_{nl} is given in Appendix A. We have introduced the characteristic frequency $\omega = \sqrt{(\gamma_1 + \gamma_2)K}$ and length $a^2 = \hbar\omega/K$ of the harmonic potential, both defined in terms of the heavy-hole mass. The energy levels of the 2D oscillator are then

$$E_{nl} = (2n + |l| + 1)\hbar\omega. \quad (13)$$

As a convenient basis set for the subband states we choose simple trigonometric functions,²¹ viz.,

$$f_s(z) = \sqrt{\frac{2}{W}} \sin\left[s\pi\left(z + \frac{W}{2}\right) / W\right]. \quad (14)$$

Strictly speaking this set is only complete on the interval $[-W, W]$ (which would be the situation if we put hard walls at $z = \pm W$). But for relatively large offsets the wave function will decay rapidly inside the barrier material. If W is chosen large enough to cover the dominant region of wave-function penetration the errors in neglecting the tail of the wave function will be exponentially small. The expansion width W could furthermore be treated as another variational parameter. However, in most cases the dominant energy term is the subband energy, and in this case a good first estimate of W can be obtained by minimizing the energy for the lowest subband. This optimum value is given by the equation

$$\frac{w}{W} = \frac{V_{\text{Off}}}{2\pi^2} [1 + \cos(\pi w/W)], \quad (15)$$

where $V_{\text{Off}} = 2mw^2\Delta E_v/\hbar^2$, w is the actual width of the quantum well, and m is the mass of the subband in question. In the limit of strong confinement the optimum expansion width W is only slightly larger than the quantum well width w , to first order given as

$$W = w(1 + 2/V_{\text{Off}}^{1/2}). \quad (16)$$

When more subbands are included in the basis the optimum expansion width should of course be increased. Having found the appropriate basis set we expand the hole wave function as

$$\psi_{f_z}^{\pm} = \sum_{j_z, n, s} C(n, s, j_z) \phi_{n, f_z - j_z, s}(\mathbf{r}) |\frac{3}{2}, j_z\rangle, \quad (17)$$

for states with even (+) or odd (-) parity and total angular momentum f_z . The twofold Kramer's degeneracy is still present of course: States with $\pm f_z$ have the same energy. We will label the states (17) by the smallest in-plane angular momentum ($|l|$) present in the expansion, indexed by f_z . Thus, states with an s -like envelope will be labeled S_{f_z} , p -like as P_{f_z} , etc.

Note that since we expand the in-plane solutions in terms of the heavy-hole (HH) oscillator states the light-hole (LH) block of the Kohn-Luttinger Hamiltonian is not diagonal in this basis. We could have chosen to expand the heavy- and light-hole states in two different oscillator sets, but such an approach would have led to matrix elements between oscillator sets of different masses. In the present formulation *all* matrix elements can be calculated analytically. For the subband states this is trivial due to the simple trigonometric form of the basis set. For the in-plane contribution this is accomplished by exploiting the fact that the off-diagonal terms R and S in the Kohn-Luttinger Hamiltonian act as raising and lowering operators for the 2D oscillator levels. All off-diagonal matrix elements can consequently be found by simple algebraic means. The same method is used to calculate the light-hole matrix elements within the heavy-hole basis. A complete account of the operator relations needed to do this is given in Appendix A.

C. Two-hole basis

We now consider two holes in the quantum dot. The Hamiltonian for this problem reads

$$H = H_{KL}(1) + H_{KL}(2) + V_{||}(\rho_1) + V_{||}(\rho_2) + V_{\perp}(z_1) + V_{\perp}(z_2) + V(1, 2), \quad (18)$$

in obvious notation. The Coulombic hole-hole interaction only affects the envelope part (in the effective-mass approximation) so a general state can be written,

$$\Psi(\mathbf{r}_1, \mathbf{r}_2) = \sum_{j_z, j_z'} F^{j_z, j_z'}(\mathbf{r}_1, \mathbf{r}_2) |\frac{3}{2}, j_z\rangle |\frac{3}{2}, j_z'\rangle. \quad (19)$$

Since the single-hole basis (11) allowed us to calculate all single-hole matrix elements analytically, we choose to expand the two-hole envelopes in products of single-hole states:

$$F(\mathbf{r}_1, \mathbf{r}_2) = \sum_{n, n'} C(n, n') \phi_n(\mathbf{r}_1) \phi_{n'}(\mathbf{r}_2). \quad (20)$$

Here n formally represents the set of quantum numbers for the hole and ϕ is the single-hole envelope.

The Coulomb interaction is invariant with respect to simultaneous rotations of both holes. Using again the axial approximation in the single-hole Hamiltonians the two-hole eigenstates will have a definite total angular momentum in

the z direction. The Bloch part contributes now an angular momentum $J_z = j_z + j_z'$, so a state with total angular momentum F_z has an orbital momentum $L_z = F_z - J_z$. Since $L_z = l_z + l_z'$, we have in general infinitely many single-hole envelopes contributing. To keep the basis finite we must therefore take $|l| \leq l_{\max}$.

To comply with the exclusion principle the expansion coefficients $C(n, n')$ must be antisymmetrized with respect to particle interchange. In the analogous electron problem, where spin-orbit interaction is negligible, the two-electron wave function can be classified as either singlet or triplet since the spatial and spin part separate. In the two-hole problem, however, such a separation is in general no longer possible due to the strong spin-orbit coupling and the complicated nature of the valence band.

By construction our product basis allows us to calculate all single-hole matrix elements analytically. The Coulomb potential is the only term that couples the two holes. With a little algebra the matrix elements of the Coulomb interaction can be related to a small number of one-dimensional integrals that are easily done numerically. (See Appendix B.) Furthermore, the Coulomb interaction is diagonal in both spin and total orbital angular momentum space. Consequently, it only couples states with the same $|\frac{3}{2}, j_z\rangle |\frac{3}{2}, j_z'\rangle$ and L_z .

III. COMPUTATIONAL DETAILS

In this section we give a brief account of the computational methods used to solve the variational problem. It is well known that the minimization of the energy with respect to the expansion coefficients translates into a matrix eigenvalue problem. For the single-hole problem a standard diagonalization technique, which provides all eigenvectors and eigenvalues, is applicable. This is simply because the number of basis functions needed is in general relatively small. In the axial approximation it is more precisely $\mathcal{N}_1 = 4 \times N \times S$, where N and S are the number of oscillator states and subband states included in the basis. So for most practical purposes a basis containing, say, 100 states is adequate.

The two-hole problem on the other hand is much more computationally demanding and requires a different approach. With the two-hole basis in Eq. (20) we see that the number of basis functions is now $\mathcal{N}_2 \approx (2l_{\max} + 1) \mathcal{N}_1^2$. To account for important correlations we need to take $l_{\max} = 2$, which means that \mathcal{N}_2 very quickly becomes beyond both computational and storage capacity of present-day computers using a brute-force diagonalization technique. Insisting on a method that is both simple to implement and still capable of handling such a large basis we turn instead to an iterative relaxation technique.

In terms of the imaginary-time parameter $\tau = it$, the τ -dependent Schrödinger equation can be written

$$-\hbar \frac{\partial \Psi}{\partial \tau} = H \Psi. \quad (21)$$

In a variational approach we expand $\Psi(\tau)$ in the basis ϕ_n for a given symmetry:

$$\Psi(\tau) = \sum_n c_n(\tau) \phi_n. \quad (22)$$

The solutions of (21) will now relax towards the lowest-energy state such that when $\tau \rightarrow \infty$,

$$\Psi(\tau) \approx \sum_n c_n(\tau) \phi_n \approx \Psi_0 e^{-E_0 \tau / \hbar} \quad (23)$$

is the best variational estimate to the ground state Ψ_0 .

The method gives the variational energy exactly only for infinitely slow relaxation. With a small, but finite time step $\Delta \tau$, the expansion coefficients follow the first-order dynamics

$$c_n(\tau + \Delta \tau) = c_n(\tau) - \frac{\Delta \tau}{\hbar} \sum_k \langle n | H | k \rangle c_k(\tau). \quad (24)$$

The relaxation technique is particularly useful in the present case as the action of the Hamiltonian on the state vector can be easily calculated. Because the Hamiltonian can be separated into a sum of single-particle Hamiltonians plus the mutual Coulomb interaction term that is block diagonalized by the total angular-momentum states, the action of the Hamiltonian on the state vector involved becomes much simpler. There is no need to store the entire Hamiltonian matrix. In the actual calculation we only store the one-dimensional integrals that enter into the calculation of the matrix elements of the Coulomb potential. The method is equivalent to the Lanczos method for solving a sparse matrix. However, the relaxation method is easier to implement.

From the dynamics of Eq. (24) we see that if the initial-state vector is chosen with a symmetry that corresponds to an irreducible representation of H , the state vector retains this symmetry during the relaxation process. Excited states with different symmetry from the ground state can therefore be found along the same lines as described above.

In the calculation the number of iterations varies with the choice of the initial wave function. The program iterates until the difference in energy between successive iterations is smaller than a prescribed tolerance (say, 0.001 meV). For the very first value of $\hbar \omega$ it takes as many as 2000 iterations to reach the tolerance. However, for the next value the previous state vector is used as the initial guess, and typically 100 iterations will suffice. So the smaller the spacing of $\hbar \omega$ is used, the smaller the number of iterations is needed.

IV. RESULTS AND DISCUSSION

In this section we present the results of the numerical calculations. We use the material parameters for GaAs listed in Ref. 22:

$$\gamma_1 = 6.85, \quad \gamma_2 = 2.1, \quad \gamma_3 = 2.9, \quad \epsilon = 13.18. \quad (25)$$

As we have already tailored our subband basis to the case of strong confinement in the growth direction we will ignore the mismatch between the Luttinger parameters in the GaAs well and the $\text{Al}_x\text{Ga}_{1-x}\text{As}$ barrier. The advantage of this approximation is that it avoids the cumbersome matching of the multicomponent wave function at the interface between two dissimilar materials. As long as the wave-function penetration into the barrier material is small, this approach should be well justified.

The depth of the quantum well is determined by the offset between the valence-band edges in the dot and the barrier

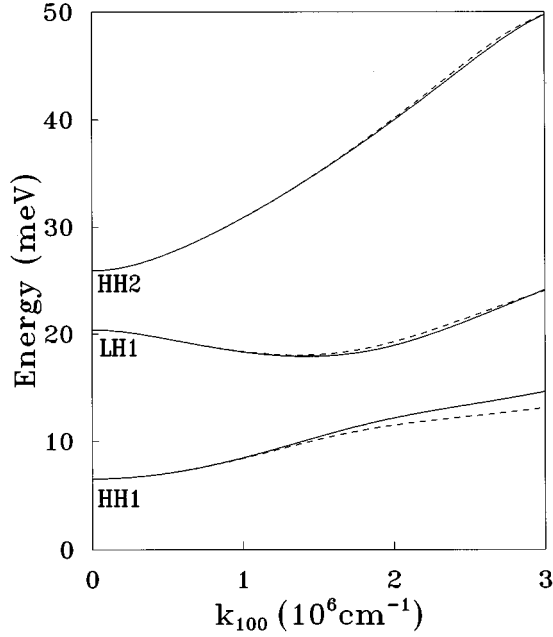


FIG. 1. The in-plane dispersion relation of a GaAs/ $\text{Al}_{0.3}\text{Ga}_{0.7}\text{As}$ [001] quantum well of thickness 100 \AA and valence-band offset $\Delta E_v = 130 \text{ meV}$ shown as a function of the wave vector K_{100} . The solid lines are the results based on the full Kohn-Luttinger Hamiltonian, while the dashed lines are obtained using the axial approximation.

materials. For the GaAs/ $\text{Al}_x\text{Ga}_{1-x}\text{As}$ interface we use the division 65/35 of the band-gap discontinuity between the conduction band and the valence band. The valence-band offset can then be estimated from the formula

$$\Delta E_v = 0.35\Delta E_g(x), \quad (26)$$

where $\Delta E_g(x)$ is the difference in band gaps for $\mathbf{k}=0$ between GaAs and $\text{Al}_x\text{Ga}_{1-x}\text{As}$. For $x < 0.45$ we take $\Delta E_g(x) = 1247x \text{ meV}$. Focusing on alloys with $x=0.3$ we thus obtain a valence-band offset $\Delta E_v = 130 \text{ meV}$.

In Fig. 1 the in-plane hole dispersion of a 100-\AA -wide GaAs/ $\text{Al}_{0.3}\text{Ga}_{0.7}\text{As}$ [001] quantum well is shown along the [100] direction. The result with and without the axial approximation is plotted. We recognize the electronlike dispersion of the light-hole subband near the zone center and note that the axial approximation works very well. In the figure we also introduce the labeling of the states, viz., HH's and LH's, where s refers to the s th subband. A few of the lowest subband edges are listed in Table I. A strict classification of states as heavy hole or light hole should be done on the basis of their in-plane dispersion, and not on the quantum number

TABLE I. The lowest subband energies for a valence-band offset $\Delta E_v = 130 \text{ meV}$. The quantum-well width w is given in \AA , and all energies are in meV.

w	HH1	LH1	HH2	HH3	LH2
100	6.52	20.36	25.87	57.27	76.99
150	3.20	10.89	12.76	28.58	42.78
200	1.89	6.75	7.57	16.99	26.79

f_z being $\pm\frac{3}{2}$ or $\pm\frac{1}{2}$.²³ However, here we still use the terminology that HH (LH) refers to the subband whose wave function is dominated by the $\frac{3}{2}$ ($\frac{1}{2}$) component near the zone center. Away from the zone center, the dominant component for a given subband may change as a result of band mixing. In this and the other figures we use the hole picture in which the energy scale is turned upside down, and we measure all energies relative to the valence band edge in bulk.

A. Single-hole energies

We want first to study the effect of the parabolic confinement potential on the single-hole states. Experiments on few-

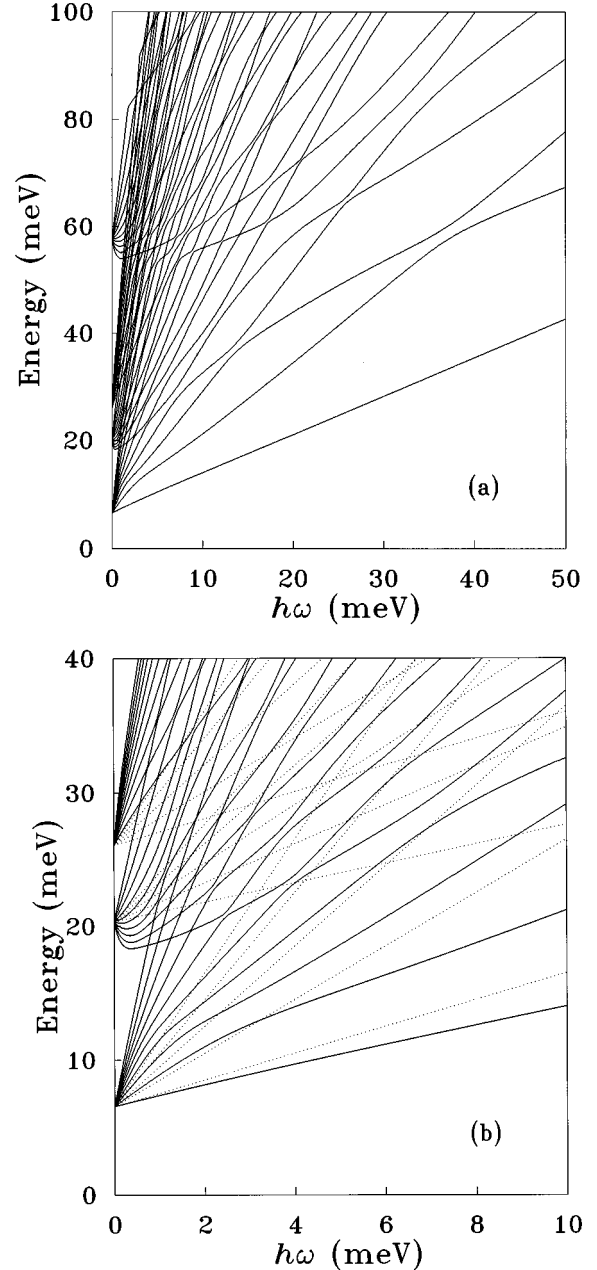


FIG. 2. (a) Energy levels of the symmetry state $S_{3/2}^+$ as a function of the confinement potential $\hbar\omega$. The quantum-well thickness is 100 \AA and the valence-band offset $\Delta E_v = 130 \text{ meV}$. The axial approximation is used in this and all subsequent figures. Note that no levels cross. (b) Energy levels (solid lines) as in (a) with some uncoupled levels indicated by the dotted lines.

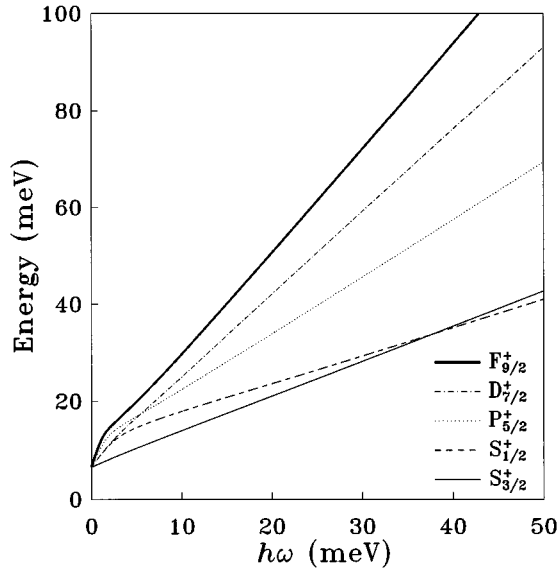


FIG. 3. The lowest energy levels for the five different symmetries $S_{3/2}^+$, $S_{1/2}^+$, $P_{5/2}^+$, $D_{7/2}^+$, and $F_{9/2}^+$. The quantum well is the same as in Fig. 2. The light-hole-like $S_{1/2}^+$ state replaces the heavy-hole-like $S_{3/2}^+$ state as the ground state for $\hbar\omega \geq 37.7$ meV.

electron systems in parabolic quantum dots suggests that the confinement potential $\hbar\omega$ typically lies in the range 1–10 meV. However, as no experimental data on holes in parabolic quantum dots are available, we allow the confinement potential to vary in a slightly larger interval. This will also allow us to make some predictions about the energy levels in the strong confinement regime.

Figure 2(a) shows some low-lying energy levels for the $S_{3/2}^+$ states. As the coupled levels of the same symmetry are forbidden to cross we see that the intersubband couplings result in strong anticrossing of the levels. In the weak confinement limit, $\hbar\omega \rightarrow 0$, the levels approach the HH1, LH1, HH2, and HH3 subband edges of the quantum well. When the strength of the potential is increased and the confinement energy becomes comparable to the subband splitting the levels couple strongly, resulting in nonlinear dependence on $\hbar\omega$. Approaching the strong confinement limit the levels regain a linear behavior, but they are still coupled. In the weak (strong) confinement limit only the R (S) coupling term in the Kohn-Luttinger Hamiltonian is relevant.²⁴ Furthermore, levels with the same linear slope will be parallel in the strong confinement limit, only shifted by a subband energy. For small confinement energy ($\hbar\omega < 0.5$ meV), the energies of

the states derived from the LH1 and HH3 subbands are found to first decrease and then increase as $\hbar\omega$ increases. This is due to the fact that these hole subbands have negative effective masses at the zone center and their subband minimum is away from the zone center (see Fig. 1), and we have used a finite number of oscillator states in the expansion. If an infinite number of oscillator states is used, we expect that all energy levels will approach the subband minimum (rather than the subband edge) as $\hbar\omega \rightarrow 0$. Thus our results are convergent only for $\hbar\omega > 0.3$ meV. Below that more oscillator states are needed in the calculation. However, since the correct results are already known for $\hbar\omega = 0$ (which are exactly the subband energies), these results can be obtained simply by interpolation between the $\hbar\omega = 0$ and $\hbar\omega = 0.3$ meV values.

Figure 2(b) is an enlarged version of Fig. 2(a) for $\hbar\omega < 10$ meV and the energy levels obtained without the off-diagonal coupling terms (dotted lines). Comparing the coupled and uncoupled levels in Fig. 2(b), we find that the effect of band coupling is quite evident. Without band coupling, all energy levels increase linearly with $\hbar\omega$, whereas the inclusion of band coupling makes some of the low-lying energy levels increase nonlinearly with $\hbar\omega$. For the ground state, although the energy appears to increase linearly, it has a smaller slope than the corresponding uncoupled level as a result of band coupling: According to the variational principle the coupling terms always lower the energy, giving the level a *weaker* dependence on the confinement potential than the corresponding uncoupled level.

Figure 3 displays the lowest energy levels for five different symmetries, viz., $S_{3/2}^+$, $S_{1/2}^+$, $P_{5/2}^+$, $D_{7/2}^+$, and $F_{9/2}^+$. We notice that the $S_{3/2}^+$ (and $D_{7/2}^+$) state appears to be almost linear in $\hbar\omega$, whereas the $S_{1/2}^+$ state crosses the $S_{3/2}^+$ state at $\hbar\omega \approx 37.7$ meV and it replaces the $S_{3/2}^+$ state as the ground state. The key to understanding the behavior in Fig. 3 is given in Table II where we show how various states are coupled in the axial approximation. From Table II we see that in the strong-confinement limit the $S_{3/2}^+$ state will be (mostly) heavy-hole-like, whereas the $S_{1/2}^+$ state will be light-hole-like. The bulk heavy- (light-) hole state has a heavy (light) effective mass in the z direction and a light (heavy) effective mass in the in-plane direction. The confinement effect due to the quantum well causes a larger energy shift for the light-hole state than for the heavy-hole state, while the in-plane confinement effect due to the quantum dot parabolic potential causes the opposite effect. The crossover from a heavy-hole-like ground state to a light-hole-like ground state

TABLE II. Subband and angular momentum states that are coupled by the off-diagonal terms in the Kohn-Luttinger Hamiltonian. We only list the lowest subband state; all higher subband states with the same parity are also coupled.

$S_{3/2}^+$		$S_{1/2}^+$		$P_{5/2}^+$		$D_{7/2}^+$		$F_{9/2}^+$	
Subband	l								
HH1	0	HH2	-1	HH2	1	HH1	2	HH2	3
LH2	1	LH1	0	LH1	2	LH2	3	LH1	4
LH1	2	LH2	1	LH2	3	LH1	4	LH2	5
HH2	3	HH1	2	HH1	4	HH2	5	HH1	6

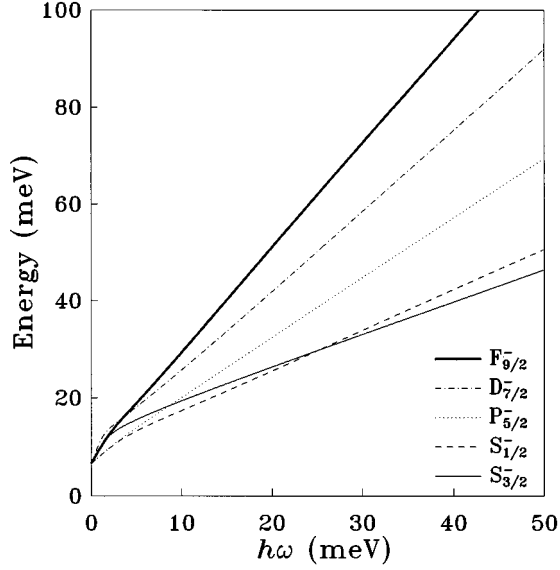


FIG. 4. Same as Fig. 3, but for the lowest energy levels with symmetry $S_{3/2}^-$, $S_{1/2}^-$, $P_{5/2}^-$, $D_{7/2}^-$, and $F_{9/2}^-$. The two lowest states, $S_{3/2}^-$ and $S_{1/2}^-$, which cross at $\hbar\omega \approx 25.2$ meV also cross at a higher energy ($\hbar\omega \approx 214$ meV, not shown in the figure). The lowest energy level is thus light-hole-like in the strong-confinement limit.

is thus associated with a crossover from quasi-two-dimensional (2D) to quasi-1D behavior. It is now also evident why the $S_{3/2}^+$ level displays the most linear behavior. This state is (mostly) HH1-like in both the weak- and strong-confinement limits. The same almost linear behavior can be found (for the same reason) for all the states $L_{L+3/2}^{(-)L}$, e.g., $S_{3/2}^+$, $P_{5/2}^-$, $D_{7/2}^+$, etc. This is exemplified in Fig. 4 where we plot the odd-parity states $S_{3/2}^-$, $S_{1/2}^-$, $P_{5/2}^-$, $D_{7/2}^-$, and $F_{9/2}^-$. We see that the states $P_{5/2}^-$ and $F_{9/2}^-$ are almost linear. The $S_{1/2}^-$ state is the lowest odd-parity state for sufficiently low $\hbar\omega$, it crosses the $S_{3/2}^-$ state at $\hbar\omega \approx 26$ meV to become the second lowest, and it eventually crosses the $S_{3/2}^-$ state again (at $\hbar\omega \approx 214$ meV, not shown in the figure), so the lowest odd-parity state also becomes light-hole-like in the strong-confinement limit.

We end this section by concluding that the levels show in general a nonlinear dependence on the confinement potential. Even in the limit of weak and strong confinement, where the levels are almost linear, the intersubband couplings cannot be entirely neglected.

B. Two-hole energies

We now consider two holes in the quantum dot. Including both the off-diagonal coupling terms in the Kohn-Luttinger Hamiltonian and the Coulomb interaction we have a demanding numerical problem. To accurately describe the two-hole system in the product basis (20) we include, for each hole, the three lowest subbands with the correct parity. In the lateral directions we use the 30 lowest oscillator states for each hole, corresponding to the different angular states with $l=0, \pm 1, \pm 2$. The total basis then consists of 9792 different functions with even parity and 9648 functions with odd parity. This is sufficient to give the energy (relative to the computed band edge) within less than 0.2 meV, except possibly

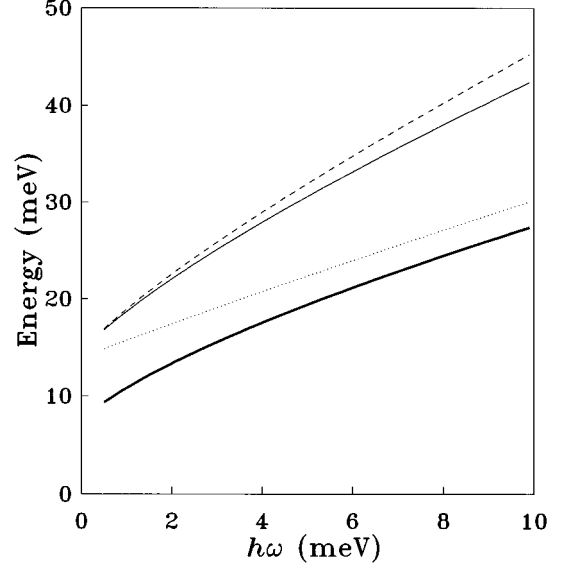


FIG. 5. The two-hole ground-state energy (thin solid line) for the state S_0^+ for a 100-Å-wide quantum well with a valence-band offset $\Delta E_v = 130$ meV. The energy is calculated using the relaxation method and the axial approximation. The dashed line is obtained ignoring all off-diagonal terms in the Kohn-Luttinger Hamiltonian, hence using a one-band model. The dotted line is the energy of two noninteracting holes (including the off-diagonal couplings in the Kohn-Luttinger Hamiltonian). The thick solid line is the resonant tunneling energy E_R as defined in Eq. (27).

in the extreme weak-confinement limit where a larger number of oscillator states is needed. However, in this limit the exact energy is already known; with no confinement potential the energy is simply twice the lowest subband energy. We make therefore no attempt to numerically calculate the two-hole energy for confinement energies below 0.5 meV and focus instead on more confined states.

To test the flexibility of our basis we have performed two mutually independent tests. First, we calculated the energy of the S_0^+ state without the Coulomb interaction and the particle statistics. We then obtained twice the single-hole energy found in Sec. IV A for the $S_{3/2}^+$ state. Second, we calculated the two-hole energy in the extreme 2D limit. In this limit a single-band theory is applicable, and our results checked with those of Merkt, Huser, and Wagner⁶ who calculated the energy of two electrons in a 2D parabolic quantum dot.

In Fig. 5 we plot the lowest two-hole energy (thin solid line) for the S_0^+ state as a function of the confinement energy for a 100-Å-wide quantum well. From the first-order estimate in Eq. (16), based on only one subband, the expansion width follows as $W = 117$ Å. Since we include three subbands, the actual expansion width used in the calculation is taken as $W = 123$ Å. In the figure we have also included, for comparison purposes, the results without the off-diagonal terms in the Kohn-Luttinger Hamiltonian (dashed line), as well as the energy of two noninteracting holes (dotted line). The exact solution always lies within these two limits. The importance of the coupling terms is evident as they lower the energy substantially. This effect is even more prominent for the other symmetries, since the dominant contribution to the two-hole state S_0^+ comes from the (almost uncoupled) single-

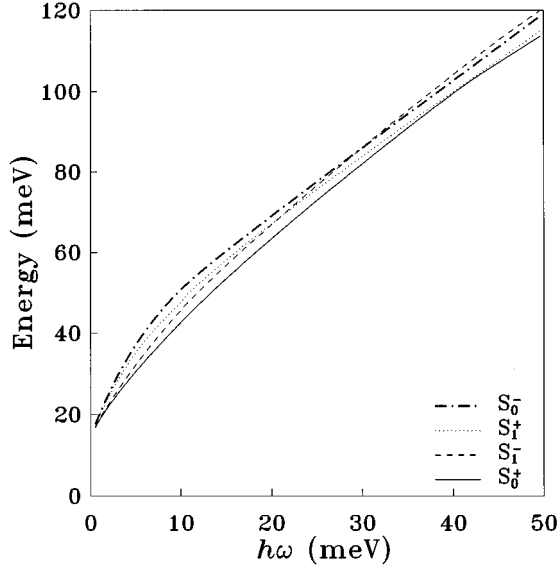


FIG. 6. The lowest two-hole energies for the four different symmetries S_0^+ , S_0^- , S_1^+ , and S_1^- . The quantum well is the same as in Fig. 5. As explained in the text the levels S_1^- and S_1^+ cross at $\hbar\omega \approx 21.5$ meV due to the inverted ordering of the single-hole states $S_{3/2}^+$ and $S_{1/2}^+$. For the same reason the two states S_0^+ and S_1^+ are energetically close at $\hbar\omega \sim 41$ meV, but S_0^+ is always the ground state.

hole states $S_{\pm 3/2}^+$ for these values of the confinement potential. As we know from the single-hole treatment, the effect of the coupling terms increases with increasing confinement, and the same trend is seen for the two-hole energy. From the figure we also notice that the effect of the Coulomb interaction is in general nonlinear with respect to the confinement potential. Consequently, the total energy cannot be written as a sum of single-particle energies plus a *constant* Coulomb charging energy. To see this more clearly we define the resonant tunneling energy for the dot E_R as

$$E_R = E(N=2) - E(N=1), \quad (27)$$

i.e., the energy difference with one and two holes in the dot. Figure 5 also includes a plot of E_R as a function of the confinement energy (thick solid line). The second hole can tunnel into the dot when the Fermi energy of the reservoir coincides with the two-hole energy level of the dot. The resonant tunneling energy is thus a measure of the gate potential needed to accomplish this. As expected E_R increases monotonically with the confinement potential, and is almost linear in the strong confinement limit (where the Coulomb potential can be considered as a perturbation).

For completeness we end this section by presenting in Fig. 6 the lowest two-hole states corresponding to the symmetries S_0 and S_1 for states of even and odd parity (see Table III). All states correspond to the ground state (lowest energy state) for the selected symmetry. The ordering of the two-hole levels in Fig. 6 can be understood qualitatively on the basis of the single-hole analysis in the previous subsection. For sufficiently weak-confinement potential we see from Figs. 3 and 4 that the ordering (increasing in energy) of the single-hole levels is $S_{3/2}^+$ and $S_{1/2}^-$. In this limit the two lowest two-hole states would thus be S_0^+ and S_1^- , respectively.

TABLE III. The various single-hole product states that couple to form the two-hole states in Fig. 6. Only the contribution from the S -like (i.e., $l=0$) single-hole envelopes is listed.

S_0^+	S_0^-	S_1^+	S_1^-
$S_{3/2}^+ S_{-3/2}^+$	$S_{3/2}^+ S_{-3/2}^-$	$S_{3/2}^+ S_{-1/2}^+$	$S_{3/2}^+ S_{-1/2}^-$
$S_{3/2}^- S_{-3/2}^-$	$S_{3/2}^- S_{-3/2}^+$	$S_{3/2}^- S_{-1/2}^-$	$S_{3/2}^- S_{-1/2}^+$
$S_{1/2}^+ S_{-1/2}^+$	$S_{1/2}^+ S_{-1/2}^-$	$S_{1/2}^+ S_{1/2}^+$	$S_{1/2}^+ S_{1/2}^-$
$S_{1/2}^- S_{-1/2}^-$	$S_{1/2}^- S_{-1/2}^+$	$S_{1/2}^- S_{1/2}^-$	$S_{1/2}^- S_{1/2}^+$

However, in the strong-confinement regime of Figs. 3 and 4 the ordering of the single-hole levels is changed to $S_{1/2}^+$ and $S_{3/2}^+$. The lowest two-hole states would now be S_0^+ and S_1^+ . The crossing of the states S_1^- and S_1^+ is seen in Fig. 6 at $\hbar\omega \approx 21.5$ meV. We also notice that although S_0^+ is always the ground state, the state S_1^+ is close in energy around $\hbar\omega \approx 41$ meV. This is not surprising since the primary components of these two-hole states, $S_{3/2}^+$ and $S_{1/2}^+$, are degenerate in energy at $\hbar\omega \approx 37.7$ meV, where the corresponding one-hole states cross (see Fig. 3). We note that the two-hole state S_0^+ is changed from a product of primarily heavy-hole like states in the weak-confinement limit to a product of primarily light-hole like states in the strong confinement limit.

V. SUMMARY

We have studied in this work single- and two-hole states in a parabolic quantum dot. The effect of the off-diagonal terms in the Kohn-Luttinger Hamiltonian has been clarified and shown to be non-negligible. The Coulomb interaction between the holes leads in general to a resonant tunneling energy that is nonlinear with respect to the dots confinement potential. Similar nonlinear behavior was also found for electrons in the calculations by Johnson and Payne.²⁶

The quantum dots studied in this paper were taken to be 100 Å wide. The dots considered experimentally in Ref. 3 were slightly wider, typically in the range 150–200 Å. From Table I we see that for such quantum dots the heavy- and light-hole splitting at $\mathbf{k}=0$ is drastically lowered, and the importance of the off-diagonal coupling terms is even greater than in the present case. Furthermore, the confinement potential required to change the symmetry of the ground state is substantially reduced.

ACKNOWLEDGMENTS

One of us (F.B.P.) is grateful to Norges Forskningsråd for financial support. He would also like to thank Y.-C. Chang's group for its hospitality during his visit. The authors acknowledge the use of computing facilities provided by the University of Illinois, Materials Research Laboratory under Contract No. NSF/DMR-89-20538.

APPENDIX A: OPERATOR RELATIONS FOR THE 2D HARMONIC OSCILLATOR

The wave functions $|n, l\rangle$ of the 2D harmonic oscillator can be written in cylindrical coordinates as

$$\Phi_{nl}(\rho, \phi) = C_{nl}(i\rho)^{|l|} e^{-\rho^2/2a^2} e^{il\phi} L_n^{|l|}(\rho^2/a^2), \quad (\text{A1})$$

with the normalization constant

$$C_{nl} = \sqrt{\frac{n!}{\pi(n+|l|)!}} \left(\frac{1}{a}\right)^{|l|+1}. \quad (\text{A2})$$

We have chosen a specific phase to simplify the operator relations. In cylindrical coordinates the operator $k_{\pm} = k_x \pm ik_y$ takes the form

$$k_{\pm} = -ie^{\pm i\phi} \left(\frac{\partial}{\partial r} \pm \frac{i}{r} \frac{\partial}{\partial \phi} \right). \quad (\text{A3})$$

Using the properties of the Laguerre polynomial it can be shown that when $l > 0$

$$ak_+|n, l\rangle = \sqrt{n}|n-1, l+1\rangle + \sqrt{n+l+1}|n, l+1\rangle,$$

$$ak_-|n, l\rangle = \sqrt{n+1}|n+1, l-1\rangle + \sqrt{n+l}|n, l-1\rangle.$$

For $l < 0$ we have

$$ak_+|n, l\rangle = \sqrt{n-l}|n, l+1\rangle + \sqrt{n+1}|n+1, l+1\rangle,$$

$$ak_-|n, l\rangle = \sqrt{n-l+1}|n, l-1\rangle + \sqrt{n}|n-1, l-1\rangle,$$

and finally for $l=0$

$$ak_+|n, 0\rangle = \sqrt{n}|n-1, 1\rangle + \sqrt{n+1}|n, 1\rangle,$$

$$ak_-|n, 0\rangle = \sqrt{n+1}|n, -1\rangle + \sqrt{n}|n-1, -1\rangle.$$

These are the relations needed to calculate the off-diagonal terms in the Kohn-Luttinger Hamiltonian.

To calculate the matrix elements of the light-hole diagonal elements we use that

$$H_l^{\parallel} = H_h^{\parallel} - \frac{\hbar^2}{m_0} \gamma_2 k_+ k_-, \quad (\text{A4})$$

where H^{\parallel} refers to the in-plane part only. The effect of the operator $k_+ k_-$ now follows directly, and its matrix elements can be calculated analytically.

APPENDIX B: COULOMB MATRIX ELEMENTS

A convenient way to calculate the Coulomb matrix elements

$$I = \left\langle n'_1 l'_1 s'_1 n'_2 l'_2 s'_2 \left| \frac{e^2}{4\pi\epsilon |\mathbf{r}_2 - \mathbf{r}_1|} \right| n_1 l_1 s_1 n_2 l_2 s_2 \right\rangle \quad (\text{B1})$$

starts by first representing everything in terms of their Fourier transforms. Equation (B1) can then be written

$$I = \frac{1}{(2\pi)^3} \int \tilde{F}_1(\mathbf{k}) \tilde{F}_2(-\mathbf{k}) \frac{4\pi}{k^2} d\mathbf{k}, \quad (\text{B2})$$

where $\tilde{F}(\mathbf{k})$ is the Fourier transform of $\langle \mathbf{r} | n' l' s' \rangle \langle n l s | \mathbf{r} \rangle$. With separable wave functions the Fourier transforms also separate, so we can write

$$\tilde{F}(\mathbf{k}) = \tilde{F}(\mathbf{p}) \tilde{f}(q), \quad (\text{B3})$$

where $\mathbf{k} = (\mathbf{p}, q)$.

Consider first the Fourier transform of the in-plane wave function. Expanding the Laguerre polynomials as

$$L_n^{|l|}(\rho^2) L_{n'}^{|l'|}(\rho^2) = \sum_{j=0}^{n+n'} A_j \rho^{2j} \quad (\text{B4})$$

the Fourier transform is readily obtained as

$$\begin{aligned} \tilde{F}(\mathbf{p}) &= -\pi i^{l-l'} e^{i(l-l')\phi_p} \frac{p^{|l-l'|}}{2^{|l-l'|}} \\ &\times \sum_{j=0}^{n+n'} A_j \alpha_j! e^{-\frac{1}{4}p^2} L_{\alpha_j}^{|l-l'|} \left(\frac{p^2}{4} \right). \end{aligned} \quad (\text{B5})$$

Here

$$\alpha_j = j + \frac{|l| + |l'| - |l-l'|}{2} \quad (\text{B6})$$

is a positive integer and p is given in units of $1/a$.

The Fourier transform of the subband functions is straightforward and yields

$$\tilde{f}(q) = \frac{4iqss' \pi^2 [e^{iq/2} (-1)^{s-s'} - e^{-iq/2}]}{[(s-s')^2 \pi^2 - q^2][(s+s')^2 \pi^2 - q^2]} \quad (\text{B7})$$

for q in units of $1/W$.

By inserting the found Fourier transforms into the inversion formula (33) the angular integral immediately gives the condition for conservation of angular momentum, viz.,

$$\int_0^{2\pi} e^{i(l_1-l'_1)\phi_p} e^{i(l_2-l'_2)\phi_p} d\phi_p = 2\pi \delta_{l_1+l_2=l'_1+l'_2}. \quad (\text{B8})$$

Next we do the dq integral in (B2). We note first that the integral vanishes unless

$$(-1)^{s_1-s'_1} = (-1)^{s_2-s'_2} \quad (\text{B9})$$

which, together with (B8), expresses parity conservation. The integral is most easily done using contour integration in the complex q plane. The pole structure of the integrand can be classified into 8 groups. Using the residue theorem the integration yields an algebraic function of p , henceforth denoted $Q(pW/a)$. Finally, we are left with one integration, which must be done numerically. Defining

$$\begin{aligned} J(\alpha_j, \alpha_k) &= \frac{1}{4^{|l-l'|}} \int_0^{\infty} p^{2|l-l'|+1} e^{-\frac{1}{2}p^2} L_{\alpha_j}^{|l-l'|} \left(\frac{1}{4}p^2 \right) \\ &\times L_{\alpha_k}^{|l-l'|} \left(\frac{1}{4}p^2 \right) Q(pW/a) dp \end{aligned}$$

the Coulomb matrix element can be expressed as

$$I = \sum_{j=0}^{n_1+n'_1} \sum_{k=0}^{n_2+n'_2} A_j A_k \alpha_j! \alpha_k! J(\alpha_j, \alpha_k), \quad (\text{B10})$$

apart from a trivial constant.

- ¹R. C. Ashoori, H. L. Stormer, J. S. Weiner, L. N. Pfeiffer, S. J. Pearton, K. W. Baldwin, and K. W. West, *Phys. Rev. Lett.* **68**, 3088 (1992).
- ²This is at least fulfilled for small electron numbers.
- ³R. C. Ashoori, H. L. Stormer, J. S. Weiner, L. N. Pfeiffer, K. W. Baldwin, and K. W. West, *Phys. Rev. Lett.* **71**, 613 (1993).
- ⁴P. L. McEuen, E. B. Foxman, U. Meirav, M. A. Kastner, Y. Meir, and N. S. Wingreen, *Phys. Rev. Lett.* **66**, 1926 (1991).
- ⁵G. W. Bryant, *Phys. Rev. Lett.* **59**, 1140 (1987).
- ⁶U. Merkt, J. Huser, and M. Wagner, *Phys. Rev. B* **43**, 7320 (1991).
- ⁷P. A. Maksym and T. Chakraborty, *Phys. Rev. Lett.* **65**, 108 (1990).
- ⁸N. F. Johnson and M. C. Payne, *Phys. Rev. Lett.* **67**, 1157 (1991).
- ⁹A. Kumar, S. E. Laux, and F. Stern, *Phys. Rev. B* **42**, 5166 (1990).
- ¹⁰W. Kohn, *Phys. Rev.* **123**, 1242 (1961).
- ¹¹L. Brey, N. F. Johnson, and B. I. Halpern, *Phys. Rev. B* **40**, 10 647 (1989).
- ¹²F. M. Peeters, *Phys. Rev. B* **42**, 1486 (1990).
- ¹³D. A. Broido and L. J. Sham, *Phys. Rev. B* **31**, 888 (1985).
- ¹⁴D. A. Broido, A. Cros, and U. Rössler, *Phys. Rev. B* **45**, 11 395 (1992).
- ¹⁵T. Darnhofer, D. A. Broido, and U. Rössler, *Phys. Rev. B* **50**, 15 412 (1994).
- ¹⁶J. M. Luttinger and W. Kohn, *Phys. Rev.* **97**, 869 (1955).
- ¹⁷We have deliberately chosen the phases of the Bloch functions so as to render all matrix elements real.
- ¹⁸A. Fasolino and M. Altarelli, in *Two-Dimensional Systems, Heterostructures, and Superlattices*, edited by G. Bauer, F. Kucher, and H. Heinrich (Springer-Verlag, New York, 1984).
- ¹⁹See e.g., M. Altarelli, U. Ekenberg, and A. Fasolini, *Phys. Rev. B* **32**, 5138 (1985).
- ²⁰The neglected cubic terms have a fourfold symmetry, and hence couple states that differ by $\Delta f_z = 4$.
- ²¹In addition to providing simple integrals, we avoid having to use continuum states in the basis.
- ²²*Semiconductors Physics of Group IV Elements and III-V Compounds*, edited by K.-H. Hellwege and O. Madelung, Landolt-Börnstein, New Series, Group III, Vol. 17, Pt. a (Springer, Berlin, 1982); *Semiconductors. Intrinsic Properties of Group IV Elements and III-V, II-VI, and I-VII Compounds*, edited by O. Madelung, Landolt-Börnstein, New Series, Group III, Vol. 22, Pt. a (Springer, Berlin, 1987).
- ²³K. J. Vahala and P. C. Sercel, *Phys. Rev. Lett.* **65**, 239 (1990); P. C. Sercel and K. J. Vahala, *Phys. Rev. B* **42**, 3690 (1990).
- ²⁴While the diagonal terms scale as $\text{const} + \hbar\omega$, the off-diagonal coupling term R (S) scales as $\sqrt{\hbar\omega}$ ($\hbar\omega$). In the strong (weak) confinement limit we can therefore neglect R (S). This is different from the 2D limit where all coupling terms are irrelevant and a one-band model is applicable.
- ²⁵At even stronger confinement energies the single-hole ordering would be $S_{1/2}^+$ and $S_{1/2}^-$, as the light-hole states are favored in this limit. The ordering of the two-hole states would then be S_0^+ and S_1^- . This regime is outside the range of Fig. 6.
- ²⁶N. F. Johnson and M. C. Payne, *Phys. Rev. B* **45**, 3819 (1992).